Numerical Forced Convection Heat Transfer, Fluid Flow and Entropy Generation Analyses of Al_2O_3-Water Nanofluid in Elliptical Channels

O. T. Olakoyejo[1*], A. O. Adelaja[1], S. M. Abolarin[2], O. O. Adewumi[1], M. O. Oyekeye[1], A. A. Oluwo[1], O. Oluwatusin[1], A. Mweigye[3]

[1]Department of Mechanical Engineering, University of Lagos, Akoka, Lagos, Nigeria
[2]Department Engineering Sciences, University of The Free State, Bloemfontein, South Africa
[3]Department of Mechanical and Manufacturing Engineering, Schulich School of Engineering, University of Calgary, Calgary, Canada

ABSTRACT: This study investigates a three-dimensional elliptical microchannel heat sink for heat dissipation in laminar forced convection. The study seeks to improve thermal performance and overcome overheating associated with excessive temperature commonly experienced in heat-generating equipment, which is beyond the temperature usually specified by the manufacturer. The objective of the study is to evaluate the heat transfer, fluid flow, and entropy generation characteristics of Al_2O_3-water nanofluid in an elliptical cooling channel. The numerical analysis is investigated on the structure experiencing constant volumetric heat generation. The parameters considered are Reynolds number of $100 \leq Re \leq 500$, nanoparticle concentration ϕ, from 0% to 4% with channel aspect ratio A_r from 1 to 3. The impacts of these parameters on the maximum temperature, heat transfer coefficient, friction factor, and volumetric entropy generation are reported. The study demonstrates that heat transfer is enhanced in the elliptical cooling channel at different aspect ratios, nanoparticle concentrations, and Reynold numbers. The results showed that as the nanoparticle concentration, channel aspect ratio, and Reynolds number (Re) increase, the maximum temperature, and total entropy generation decrease. As the channel aspect ratio increases at a specified Re = 200 and nanofluid concentration, ϕ = 3%, the maximum temperature, and total entropy generation decrease by up to 62% while the heat transfer coefficient increases by up to 78% and the friction factor increase by less than 2% with aspect ratio. However, the friction factor is not sensitive to the nanofluid concentration as a coolant.

KEYWORDS: Forced convection, Laminar flow, Maximum temperature, Heat transfer coefficient, Entropy generation rate, Nanofluid.

[Received Jul. 14, 2022; Revised Sep. 13, 2022; Accepted Sep. 27, 2022] Print ISSN: 0189-9546 | Online ISSN: 2437-2110

NOMENCLATURE

A	Cross-sectional area (m^2)
A_r	Channel aspect ratio
Be	Bejan number
C_P	Specific heat at constant pressure (J/kg K)
d_h	Hydraulic diameter (m)
H	Structure height (m)
h	Elemental height (m)
h	Average heat transfer coefficient (W/m^{2}K)
k	Thermal conductivity (W/mK)
L	Channel length (m)
n	Normal
P	Pressure (Pa)
P	Wet perimeter (m)
$\dot{q}''$	Heat flux (W/m^2)
$\dot{q}_s'''$	Internal heat generation (W/m^3)
Re	Reynolds number
$\dot{S}_g'''$	Volumetric entropy generation rate (W/m^3.K)
T	Temperature (°C)
T_w	Area-weighted average wall temperature (°C)
$\vec{u}$	Velocity vector (m/s)
V	Global structure volume (m^3)
$\dot{V}$	Volumetric flow rate (m^3/s)
W	Structure width (m)
W	Elemental width (m)
x, y, z	Cartesian coordinates (m)
Δ	Difference
∇	Differential operator
γ	Convergence criterion
μ	Viscosity (kg/m.s)
ρ	Density (kg/m^3)
ϕ	Nanoparticle concentration (% vol.)

Subscripts

bf	Base fluid
C	Channel
el	Element
f	Fluid
fr	Friction
i	Mesh iteration index
In	Inlet
Max	Maximum, peak
nf	Nanofluid
P	Particle
S	Solid
th	Thermal
W	Wall

*Corresponding author: oolakoyejo@unilag.edu.ng
doi: http://dx.doi.org/10.4314/njtd.v19i4.9

I. INTRODUCTION

The thermal management of heat-generating equipment is a major concern to the thermal engineering community. These equipment need to be maintained and cooled at a specified temperature to avoid thermal stresses that may lead to the failure of the system. Again, space management for the arrangement of the cooling channel within the available space that will bring about effective cooling has been demonstrated by Tuckerman and Pease (1981) when they first introduced the use of a microchannel heat sink. Since then, different analytical, numerical, and experimental analyses have been conducted in this area by several researchers to understand and improve the cooling of electronic equipment.

Jing *et al*. (2018) numerically and theoretically analyzed flow boundary slip in different elliptical microchannel heat sinks to examine the thermal and size dependency of hydraulic resistance. The authors reported that thermal enhancement is a function of geometry and boundary slip. Muzychka (2007) used the intersection of the asymptotes method to design and optimize different cooling channel shapes in a laminar heat transfer. The study established that the maximum heat transfer rate density increased. Salimpour *et al*. (2018) numerically studied and designed multilayer microchannel heat sinks and discovered that the peak temperature was reduced by using three layers of the microchannel. Mardani and Salimpour (2016) studied numerically and theoretically the geometrical optimization of isosceles triangular microchannels. Their results showed that a microchannel with a side angle of 60º performed best.

However, nanofluids have been widely used in several thermal systems as working fluids due to their superior thermophysical properties over conventional fluids (Siginer and Wang, 1995, Choi and Eastman, 1995, Lee *et al*., 1999, Wang *et al*., 1999, Teng *et al*., 2010, Palm *et al*., 2006, Das *et al*., 2003, Li *et al*., 2008, Xuan and Li, 2003, Nguyen *et al*., 2007, Kalteh *et al*., 2012). Nanofluids were first proposed by Choi and Eastman (1995), followed by other authors like Lee *et al* (1999), Wang *et al* (1999) and Siginer and Wang (1995) that considered nanofluid of high thermal conductivity and added the nanofluid to conventional fluids. Experimental analyses were carried out on the behaviour and effect of Al_2O_3-water nanofluid in a microchannel by some researchers (Nguyen *et al*, 2007, Kalteh *et al*, 2012, Chein and Chuang, 2007). It was revealed that the thermal conductivity was enhanced. Hajmohammadi and Toghraei (2018) numerically designed a two-layered microchannel heat sink under non-uniform temperature distribution using nanofluid as the coolant. It was shown that thermal resistance decreased. Shi *et al*. (2018) numerically examined the thermal and fluid flow performance in a microchannel using Al2O3-water nanofluid. It was established that the heat transfer improved as nanoparticle concentration increased. Also, the influence of Al2O3-water nanofluid in a manifold microchannel was investigated, and heat transfer was enhanced as the nanoparticle concentration and inlet velocity increased (Yue *et al*., 2015).

Furthermore, to achieve better cooling channel performance, there is a need to reduce irreversibility (Zhang *et al*., 2022, Abbas *et al.*, 2020, Fadodun *et al*., 2022). Entropy generation as a measure of the degree of irreversibility in the system has been studied by many researchers. For example, Awad (2015) reviewed the impact of different nanofluids on entropy generation in microchannel heat sink performance. Alfaryjat *et al.* (2016) and Alfaryjat *et al*. (2018) investigated the impact of nanofluids on the heat transfer and entropy generation analysis in circular, square and hexagonal microchannels with uniform heat fluxes. The authors observed that nanofluid enhanced the performance of microchannels. Ebrahimi *et al* (2016) studied entropy generation using Al2O3 and CuO-water nanofluids in a microchannel incorporated with longitudinal vortex generators. They observed that nanofluids reduced irreversibility. Bahiraei and Heshmatian (2018) numerically assessed the effect of hybrid nanofluid on heat transfer, flow, and entropy generation in a microchannel, and it was found that the cooling uniformity improved. Manay *et al*. (2018) studied the entropy generation of TiO2-water nanofluid in a cooling channel. The results indicated that the thermal entropy generation rate was reduced, but the frictional entropy generation increased as the nanoparticle concentration, and Reynolds number increased. Bianco *et al*. (2014) investigated the turbulent heat transfer performance of nanofluid in mini-channels at constant wall temperature. The study found that the heat transfer rate was higher and there was a very small rise in pressure drop.

In the evaluation of entropy generation of Al2O3-water nanofluid of laminar heat transfer in mini- and microchannels, it was revealed that the total entropy generation rate increased due to an increase in frictional irreversibility (Wei Ting *et al*., 2016, Hassan *et al*., 2013). Yang and colleagues (Yang *et al*., 2005) numerically examined and optimized the entropy generation of nanofluid in a trapezoidal microchannel. They concluded that the maximum thermal entropy generation was achieved at the bottom of the channel.

In this present study, the three-dimensional simulation of forced convection of Al2O3-water nanofluid in an elliptical microchannel is conducted. The study is motivated by the quest to demonstrate that a cooling channel geometry enhances heat transfer (Meyer *et al.*, 2012, Olakoyejo, 2012, Olakoyejo *et al*., 2012a, Olakoyejo *et al*., 2012b). The aim is to examine the impact of nanofluid on heat transfer enhancement in the elliptical cooling channel at different aspect ratios and Reynolds number (Re) by cooling hotspots so that peak temperature is reduced inside the heated volume.

II. COMPUTATIONAL MODEL

Figure 1(a) illustrates the physical configuration of an elliptical cooling channel with a solid body of silicon material and the internal heat generation of 10^8 W/m^3. The coolant circulating through the channel removes heat from the hotspot of the solid by conjugate heat transfer. The fluid is considered homogenous, single-phase, laminar, steady, incompressible, and Newtonian at low pressure conditions. The symmetry advantage is used to select an elemental volume, as presented in Figure 1 (b). The selected domain consists of an elemental channel and the surrounding wall.

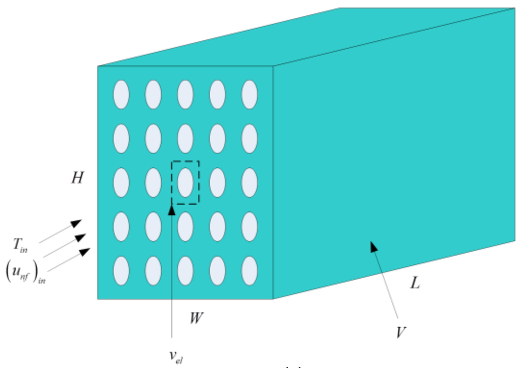

(a)

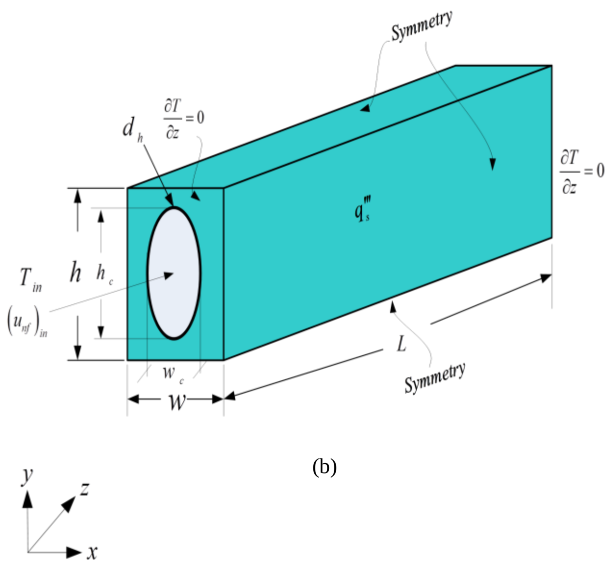

(b)

Figure 1: The (a) configuration of the elliptical cooling channels (b) elemental volume microchannel.

Table 1 presents the dimension of the elemental width, elemental height, length of a solid body, and hydraulic diameter of the channel used, as suggested by Alfaryjat *et al.* (2016).

Table 1. Dimension of the elemental volume of elliptical configuration.

d_h (μm)	W (μm)	h (μm)	L (μm)
278	788	1,500	10,000

The aspect ratio (A_r) range is $1 \le A_r \le 3$. A special case of an elliptical channel where $A_r = 1$ is a circular channel. The fluid inlet temperature is 300 K. The Reynolds number (Re) varies between 100 - 500. The nanoparticle concentration (ϕ) range is $0\% \le \phi \le 4\%$, where $\phi = 0\%$ is base fluid (water) without nanoparticle concentration.

The elemental volume, v_{el}, defined as in Eqn. 1:

$$v_{el} = whL \quad (1)$$

The elliptical channel aspect ratio was determined as in Eqn. 2:

$$A_r = \frac{h_c}{w_c} \quad (2)$$

The unit elliptical channel volume was determined as in Eqn. 3:

$$v_c = \frac{\pi}{4} h_c w_c L \quad (3)$$

where, w_c = minor diameter and h_c = major diameter.
The hydraulic diameter (d_h) was determined as in Eqn. 4:

$$d_h = 4\frac{A_c}{P_c} \quad (4)$$

where

$$A_c = \frac{\pi}{4} h_c w_c$$

The circumference of an elliptical channel was determined as in Eqn. 5:

$$P_c = \pi \left(\frac{4\left(h_c^{\,2} + w_c^{\,2}\right) - \left(h_c - w_c\right)^2}{8} \right)^{1/2} \quad (5)$$

III. GOVERNING EQUATIONS AND BOUNDARY CONDITIONS

A. *Governing Equations*

The governing differential equations used for the numerical analysis are expressed as follows:

Continuity equation:

$$\nabla \cdot \vec{u} = 0 \quad (6)$$

Momentum equation:

$$\rho_{nf}\left(\vec{u} \cdot \nabla \vec{u}\right) = -\nabla p + \mu_{nf} \nabla^2 \vec{u} \quad (7)$$

Energy equation:

$$\rho_{nf} C_{Pnf}\left(\vec{u} \cdot \nabla T\right) = k_{nf} \nabla^2 T \quad (8)$$

$$k_s \nabla^2 T + q_s''' = 0 \quad (9)$$

B. *Boundary Conditions*

The flux between the solid-liquid interfaces was determined as in Eqn. 10:

$$k_s \left.\frac{\partial T}{\partial n}\right| = k_{nf} \left.\frac{\partial T}{\partial n}\right| \quad (10)$$

The fluid velocity at the channel wall was expressed as in Eqn. 11 to be:

$$\vec{v} = 0 \quad (11)$$

while the conditions at the inlet were expressed as in Eqns. (12) and (13):

$$T = T_{in} \tag{12}$$

$$\left(u_{nf}\right)_{in} = \frac{\mathrm{Re}\,\mu_{nf}}{\rho_{nf} d_h} \tag{13}$$

Re describes the laminar flow, and the outlet condition is pressure atmosphere

The solid body boundaries,

$$\nabla T = 0 \tag{14}$$

IV. NANOFLUID THERMO-PHYSICAL PROPERTIES

Eqns. (15) to (18) were used to calculate the thermo-physical properties of the Al2O3-water nanofluid taken at 300 K (Belhadj *et al.*, 2018, Vajjha and Das, 2009, Pak and Cho, 1998).

The density was determined using Eqn. 15:

$$\rho_{nf} = (1-\phi)\rho_{bf} + \phi\rho_p \tag{15}$$

The specific heat capacity was determined using Eqn. 16:

$$\left(\rho c_p\right)_{nf} = (1-\phi)\left(\rho c_p\right)_{bf} + \phi\left(\rho c_p\right)_p \tag{16}$$

The dynamic viscosity was determined using Eqn. 17:

$$\mu_{nf} = \frac{1}{(1-\phi)^{2.5}}\mu_{bf} \tag{17}$$

The thermal conductivity was determined using Eqn. 18:

$$k_{nf} = k_{bf}\left(\frac{\left(k_P + 2k_{bf}\right) - 2\phi\left(k_{bf} - k_P\right)}{\left(k_P + 2k_{bf}\right) + \phi\left(k_{bf} - k_P\right)}\right) \tag{18}$$

V. PERFORMANCE CRITERIA

The criteria used to calculate the performance of the cooling channel are expressed below:

A. Maximum Wall Temperature

The thermal enhancement of the cooling channel is measured by the maximum temperature T_{max} experienced at the wall hotspot. A decreased maximum temperature across any hotspot surface is highly preferred for thermal performance (Tsuda *et al.*, 2017).

B. Heat Transfer Coefficient

The average heat transfer coefficient, (*h*), characterizes the improvement of heat transfer, was also considered and expressed as in Eqn. 19:

$$h = \frac{\dot{q}_s''' L}{\left(T_w - T_{in}\right)} \tag{19}$$

C. Friction Factor

The friction factor (*f*), which is also one of the criteria for measuring microchannel performance, was calculated, and it was expressed as:

$$f = \frac{2\Delta P d_h}{\rho u_{nf}^{\;2} L} \tag{20}$$

D. Entropy Generation

Another criterion of interest considered in this study that is of practical importance is the total volumetric entropy generation rate $\left(\dot{S}'''_{g-Total}\right)$ which characterizes the irreversibility of a process is expressed as (Alfaryjat *et al.*, 2016):

$$\dot{S}'''_{g-Total} = \dot{S}'''_{g-th} + \dot{S}'''_{g-fr} \tag{21}$$

Where $\dot{S}'''_{g-th}$ and $\dot{S}'''_{g-fr}$ are expressed in Eqns. (22) and (23), respectively as:

$$\dot{S}'''_{g-th} = \frac{\mu_{nf}}{T^2}\left[\left(\frac{\partial T}{\partial x}\right)^2 + \left(\frac{\partial T}{\partial y}\right)^2 + \left(\frac{\partial T}{\partial z}\right)^2\right] \tag{22}$$

$$\dot{S}'''_{g-fr} = \frac{\mu_{nf}}{T}\left\{2\left[\left(\frac{\partial u}{\partial x}\right)^2 + \left(\frac{\partial v}{\partial y}\right)^2 + \left(\frac{\partial w}{\partial z}\right)^2\right] + \left(\frac{\partial v}{\partial x} + \frac{\partial u}{\partial y}\right)^2 + \left(\frac{\partial w}{\partial x} + \frac{\partial u}{\partial z}\right)^2 + \left(\frac{\partial v}{\partial z} + \frac{\partial w}{\partial y}\right)^2\right\} \tag{23}$$

Again, the Bejan number (*Be*) is used to evaluate the thermodynamic enhancement of thermal equipment for the contributions of $\dot{S}'''_{g-th}$ and $\dot{S}'''_{g-fr}$ in total irreversibility. This dimensionless number (*Be*) is expressed as (Alfaryjat *et al.*, 2018, Alfaryjat *et al.*, 2016):

$$Be = \frac{\dot{S}'''_{g-th}}{\dot{S}'''_{g-Total}} \tag{24}$$

VI. NUMERICAL SOLUTION

A. Numerical Technique

A commercial computational fluid dynamics three-dimensional package called ANSYS FLUENT code (ANSYS) based on the finite volume method, as detailed by Patankar (1980), is employed for the numerical simulation. A SIMPLE approach is used for pressure-velocity coupling, and second-order upwind technique is used to solve the governing equations. The solution converges when the normalized residuals of the mass and momentum equations are less than 10^{-8} and the energy equation is below 10^{-12}.

B. Grid Independence Test

Numerous grid tests were conducted to guarantee the simulation results' accuracy. The convergence criterion was determined using Eqn. 25:

$$\gamma = \frac{\left|\left(T_{\max}\right)_i - \left(T_{\max}\right)_{i-1}\right|}{\left|\left(T_{\max}\right)_i\right|} \le 10^{-3} \tag{25}$$

The *i*-1 mesh is selected as Eqn. (25) is fulfilled. Table 2 indicates the grid independence test for the elliptical channel. The computational number of nodes and elements of 240,768 and 224,378, respectively, fulfilled the convergence criterion and any increase had an insignificant influence on the result.

Table 2: Grid independence study for the elliptical channel.

$L = 0.01\ m$, $w = 788\ \mu m$, $h = 1500\ \mu m$ $w_c = 100\ \mu m$, $h_c = 200\ \mu m$, $\phi = 1\ \%$ and $Re = 500$			
Number of nodes	Number of elements	$T_{max}\left({}^{0}C\right)$	γ
224100	209192	35.81	-
229080	213495	35.87	0.0018120
240768	224378	35.89	0.0004261
242478	225742	35.92	0.0008522

C. Numerical Code Validation

Figure 2 shows the validation of our numerical code compared with the past work of Alfaryjat *et al.* (2016) with circular microchannel at $q'' = 200kW/m^2$ and $200 \leq Re \leq 1680$. The results show the same trend and error deviation below 3%.

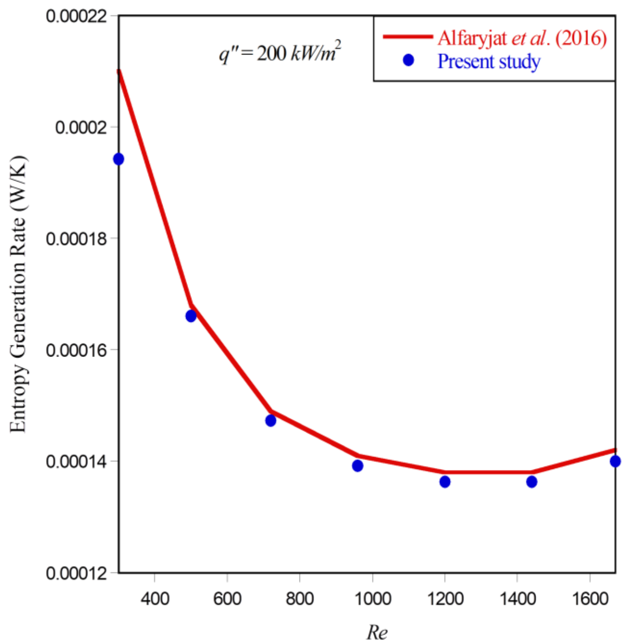

Figure 2: Validation of the present study with the work of Alfaryjat *et al* (2016)

VII. RESULTS AND DISCUSSION

A. Influence of Nanofluid Concentration, Aspect Ratio, and Reynolds Numbers on Maximum Wall Temperature

Figure 3 shows the influence of nanoparticle concentration, aspect ratio, and Reynolds number on maximum wall temperatures experienced by the elemental volume of the solid body.

Figure 3(a) showed that for the cooling channel of fixed Re, the maximum temperature monotonically decreases as the nanoparticle concentration increases. It also reveals that as the aspect ratio, Ar, increases, the maximum temperature decreases. This means that the aspect ratio, Ar, enhances the proper mixing of the fluid and reduces the thermal boundary layer thickness. Figure 3(b) shows the graph of the maximum temperature as a function of the Reynolds number for varying nanofluid concentration and at a constant aspect ratio of Ar = 2. As shown in Figure 3(b), at a fixed Ar = 2, the maximum wall temperature monotonically reduces as the Re and increase.

Therefore, the risk of hotspot formation that is damaging to the lifetime and performance of the entire system is reduced.

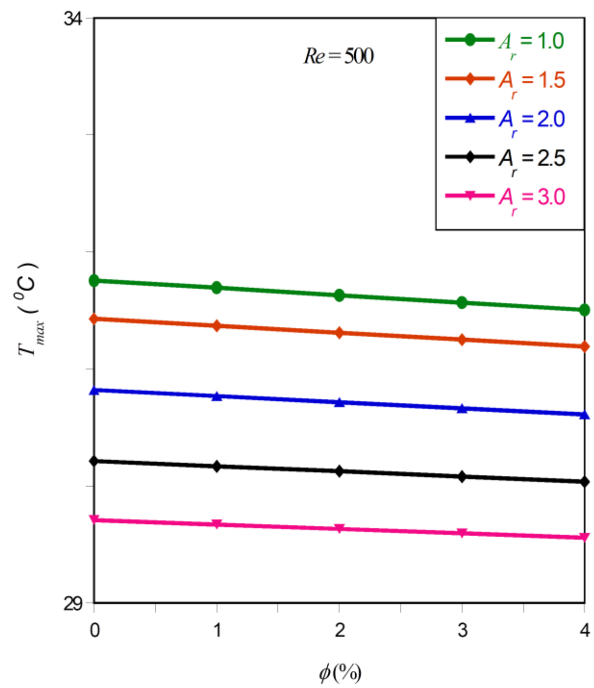

(a)

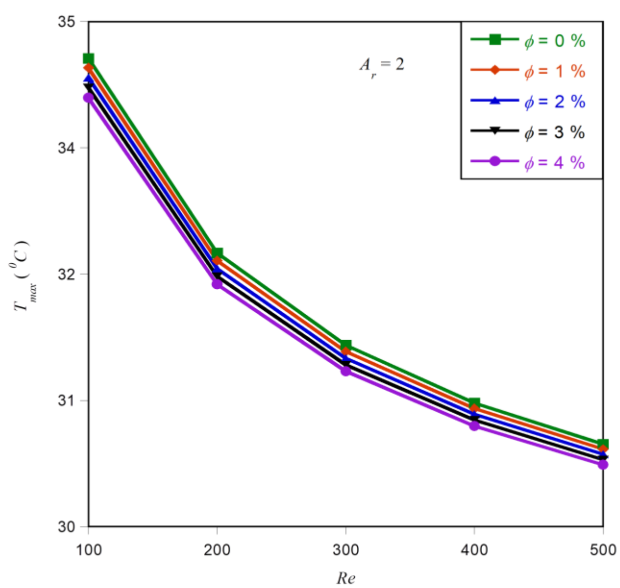

(b)

Figure 3: Effect of (a) ϕ at fixed Re = 500 and different A_r and (b) Re at fixed A_r = 2 and different ϕ on maximum wall temperature.

B. *Influence of Nanofluid Concentration, Aspect Ratio, and Reynolds Number on the Convective Heat Transfer Coefficient*

Figure 4 reveals the average heat transfer coefficient (*h*) as a function of nanofluid concentration ϕ and aspect ratio, A_r, at different *Re*. Figure 4(a) shows that for a fixed A_r = 2, the heat transfer coefficient is enhanced as the *Re* and ϕ increase. At the *Re* of 200, the heat transfer coefficient with no nanofluid fluid particle was 218870 W/m^{2}K, as the nanofluid concentration of the Al_2O_3-water was increased to 1%, the value of *h* increased to 222070 W/m^{2}K. The corresponding heat transfer coefficient increases to 225380, 228800, and 232320 W/m^{2}K as the ϕ increases to 2%, 3%, and 4%, respectively. Furthermore, at the *Re* of 500, the corresponding values of *h* for the ϕ values of 1%, 2%, 3%, and 4% are 335670, 340890, 346270, and 351810 W/m^{2}K, respectively. This signifies that an increase in the nanofluid concentration from 1% to 4% increases the value of *h* by 4.68% at the *Re* of 200 and 4.81% at the *Re* of 500. This increase in the heat transfer coefficient of the Al_2O_3-water nanofluid concentration is attributed to the increase in thermal conductivity (Lodhi *et al.*, 2020). This indicates that the maximum heat transfer coefficient as compared with water (no nanofluid) when A_r = 2 is 6.42 % and is obtained at the *Re* of 500.

Figure 4(b) reveals the heat transfer coefficient as a function of the *Re* for different values of aspect ratio and at fixed ϕ = 0.3. For a fixed ϕ = 0.3, the heat transfer coefficient increases as the A_r and *Re* increase. When *Re* is 200, and at the A_r of 1.0, the value of *h* is 180490 W/m^{2}K. The *h* increases to 228800 W/m^{2}K and 320780 W/m^{2}K when the A_r is increased to 2.0 and 3.0, respectively. As the *Re* increases to 300, the value of *h* is 217970 W/m^{2}K at the A_r of 1.0. While at the same *Re* of 300, the *h* increases to 274820 W/m^{2}K when the value of A_r is 2.0 and then increases to 383370 W/m^{2}K when the A_r is 3.0. At the value of A_r of 1.0 and the *Re* of 500, the value of *h* is obtained as 275910 W/m^{2}K. This value of *h* increases to 346270 W/m^{2}K when the value of A_r is increased to 2.0 and then to 479690 W/m^{2}K when the value of A_r is increased to 3.0. At the *Re* of 200, results show that the heat transfer coefficient increases by 26.77% as A_r is increased from 1.0 to 2.0 and 77.73% when A_r is increased from 1.0 to 3.0. Similarly, at the value of *Re* of 500, the heat transfer coefficient increases by 73.86% when the A_r increases from 1.0 to 3.0 and 38.53% when the A_r is increased from 2.0 to 3.0. This indicates that the ϕ, A_r and *Re* have strong influence and enhance the thermal performance of the cooling channel because of increased heat transfer surface area.

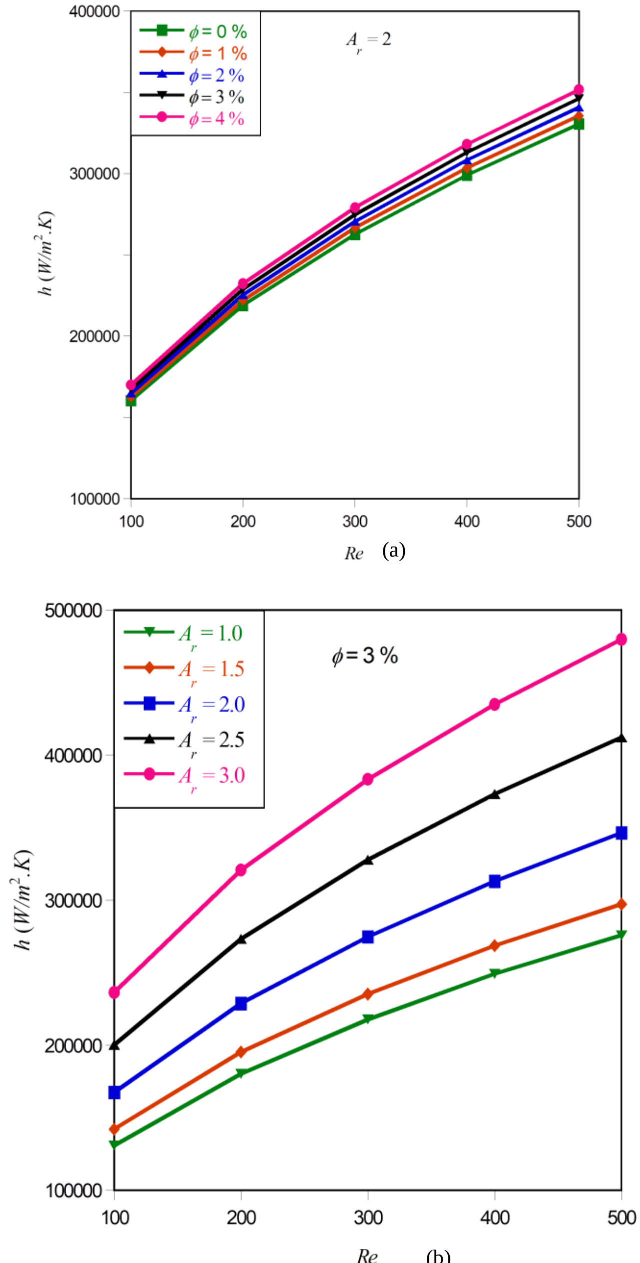

Figure 4: Effect of *Re* on *h* at fixed (a) $A_r = 2$ and different ϕ and (b) $\phi = 3\%$ and different A_r

C. *Influence of Nanofluid Concentration, Aspect Ratio, and Reynolds Number on the Entropy Generation (Thermal, Friction, and Total)*

Figure 5 shows that for a specified *Re* = 500, as the ϕ and A_r increase, the $\dot{S}'''_{g-th}$ (Figure 5(a)) and $\dot{S}'''_{g-Total}$ (Figure 5(b)) decrease, and the $\dot{S}'''_{g-fr}$ (Figure 5(a)) increases due to the increase in thermal conductivity and viscosity of the nanofluid and the aspect ratio of the elliptical configuration that provides homogenous fluid mixing. Figure 5 also discloses that the influence of $\dot{S}'''_{g-th}$is more significant than that of $\dot{S}'''_{g-fr}$ince a large portion of the $\dot{S}'''_{g-th}$ generated happens in the fluid part (Ebrahimi *et al.*, 2016).

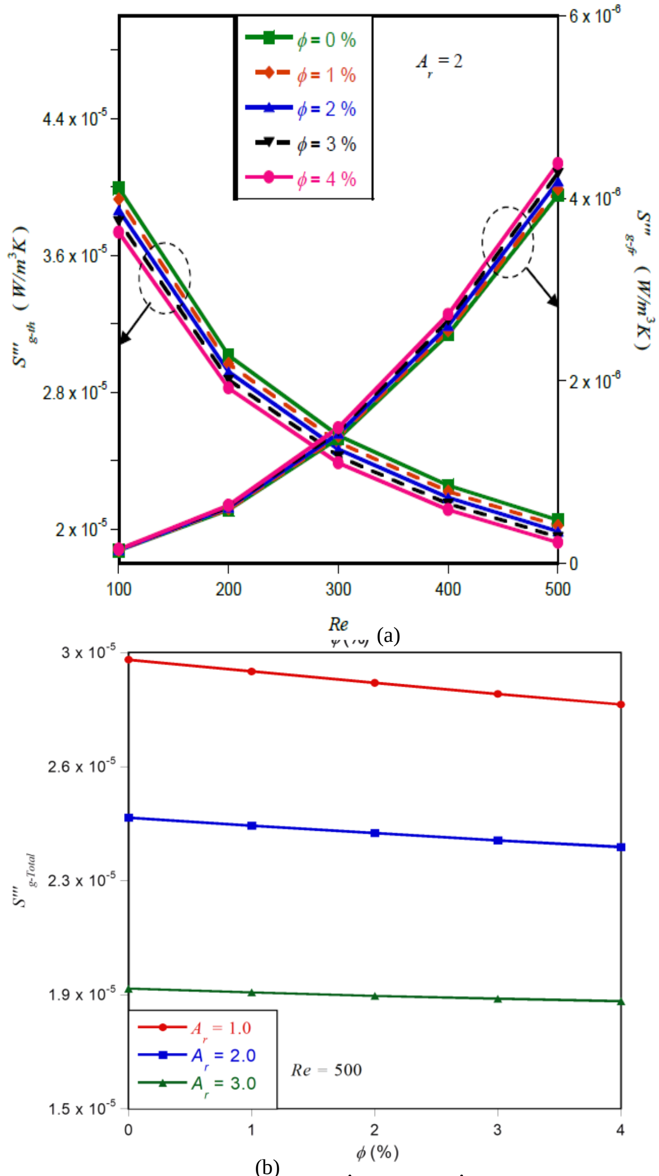

Figure 5: Effect of ϕ on (a) $\dot{S}'''_{g-th}$ and $\dot{S}'''_{g-fr}$ and (b) $\dot{S}'''_{g-Total}$ at different A_r and fixed Re = 500.

Figure 7 reveals that for a fixed A_r = 2, $\dot{S}'''_{g-th}$ and $\dot{S}'''_{g-Total}$ decrease and $\dot{S}'''_{g-fr}$ increases as the *Re* and ϕ increase. Figure 7(a) shows that at ϕ = 2%, the $\dot{S}'''_{g-th}$ decreased from 3.8643 × 10^{-5} W/m^{3}K to 2.9208 × 10^{-5} W/m^{3}K as the *Re* increases from 100 to 200. The stepwise decrease of $\dot{S}'''_{g-th}$ with *Re* increase of 300, 400, and 500 are 2.4663 × 10^{-5} W/m^{3}K, 2.1838 × 10^{-5} W/m^{3}K, and 1.9874 × 10^{-5} W/m^{3}K, respectively. However, the $\dot{S}'''_{g-th}$ decreases with an increase in the value of ϕ. On the other hand, the $\dot{S}'''_{g-fr}$ indicates a very slight increase when *Re* = 100 as ϕ increases. This shows the low *Re* of 100 could not cause a significant increase in the $\dot{S}'''_{g-fr}$.

However, as the value of *Re* increases, as shown in Figure 7(a), the difference in the values of $\dot{S}'''_{g-fr}$ increases. For instance, when the *Re* is 300, the values of $\dot{S}'''_{g-fr}$ increases as the nanofluid concentration increases from 0% to 4% with a 1% increment of ϕ to be 1.3714 × 10^{-6} W/m^{3}K, 1.3947 × 10^{-6} W/m^{3}K, 1.4218 × 10^{-6} W/m^{3}K, 1.4529 × 10^{-6} W/m^{3}K, and 1.488 × 10^{-6} W/m^{3}K, respectively. This also indicates that as $\dot{S}'''_{g-Total}$ decreases, the thermodynamic performance is enhanced in the entire system due to the use of nanofluid as coolant and A_r of the elliptical cooling channel.

Similarly, Figure 7(b) indicates a reduction in the $\dot{S}'''_{g-Total}$ as *Re* increases as well as with an increase in ϕ. The working fluid without nanofluid shows the highest $\dot{S}'''_{g-Total}$. The value of $\dot{S}'''_{g-Total}$ then increases as the concentration of nanofluid particles increases in the working fluid. Also observed is that there is a reduction in the difference in $\dot{S}'''_{g-Total}$ as the *Re* reduces. For example, at *Re* = 100, the difference in $\dot{S}'''_{g-Total}$ between the base fluid and the working fluid with a concentration of 4% is 2.558 × 10^{-6} W/m^{3}K, while at the *Re* of 500, the reduction is 9.68 × 10^{-7} W/m^{3}K. This reduction is significantly important for achieving an improved thermohydraulic cooling performance (Dong, 2019, Cai *et al.*, 2020).

D. *Influence of Re and A_r on Bejan Number*

Figure 7 illustrates Bejan number (Be) as a function of Re for different ϕ and A_r and the relative contribution of the $\dot{S}'''_{g-th}$ and $\dot{S}'''_{g-fr}$ to the $\dot{S}'''_{g-Total}$. Figure 7(a) revealed that at a specified *Re*, *Be* decreases as the ϕ increases and sharply decreases as the aspect ratio increases.

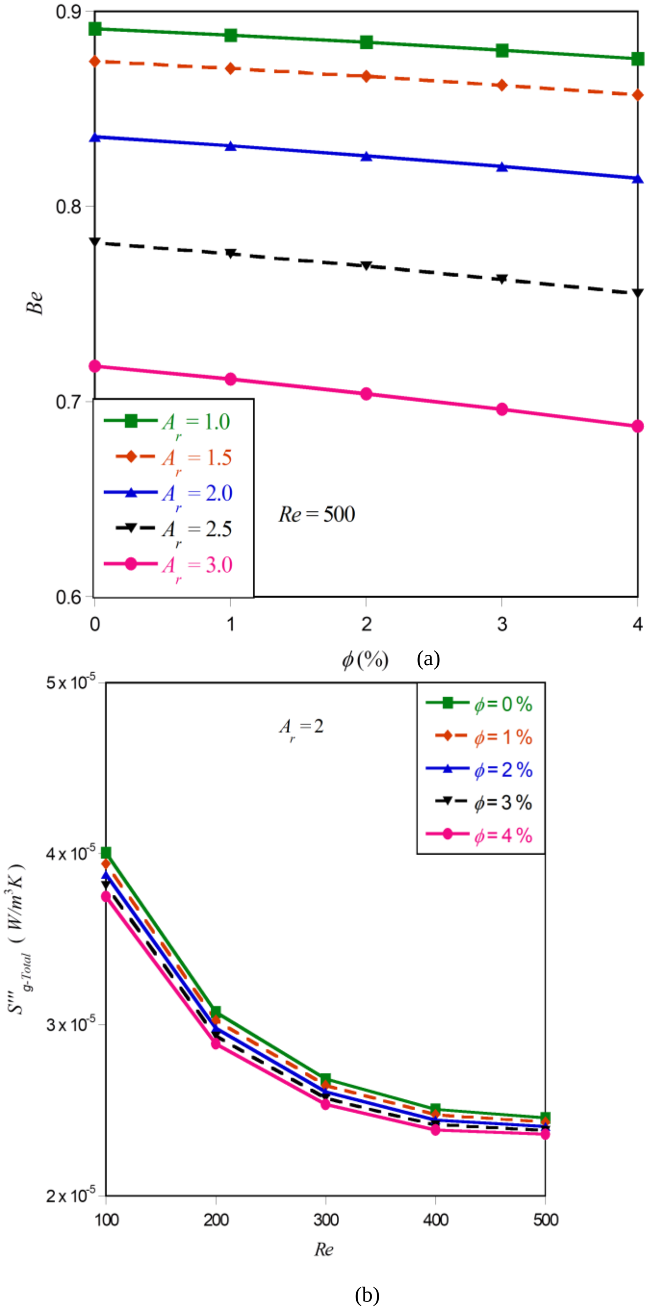

Figure 7: Effect of *Re* on (a) $\dot{S}'''_{g-th}$ and $\dot{S}'''_{g-fr}$ at fixed A_r = 2 and different ϕ and (b) *Re* on total $\dot{S}'''_{g-Total}$ at fixed A_r = 2 and different ϕ

Figure 7(b) showed that for a given A_r, *Be* decreases as the and Re increase. Figure 7(b) also revealed that an increase in Re influences the *Be* gap between the base fluid and as the increases. For instance, at the *Re* = 100, there is no significant difference between the *Be* of the base fluid and working fluid compositions. However, as the *Re* increases to 200, the difference between the *Be* of the base fluid and that of the nanofluid with 4% concentration is 0.00297. Further, an increase in *Re* to 500 increases this difference to about 0.02126. It is pertinent to highlight that the impact of the is dominant and higher than that of the for the ranges of parameters considered as the value of Be > 0.5, as shown in Figure 7.

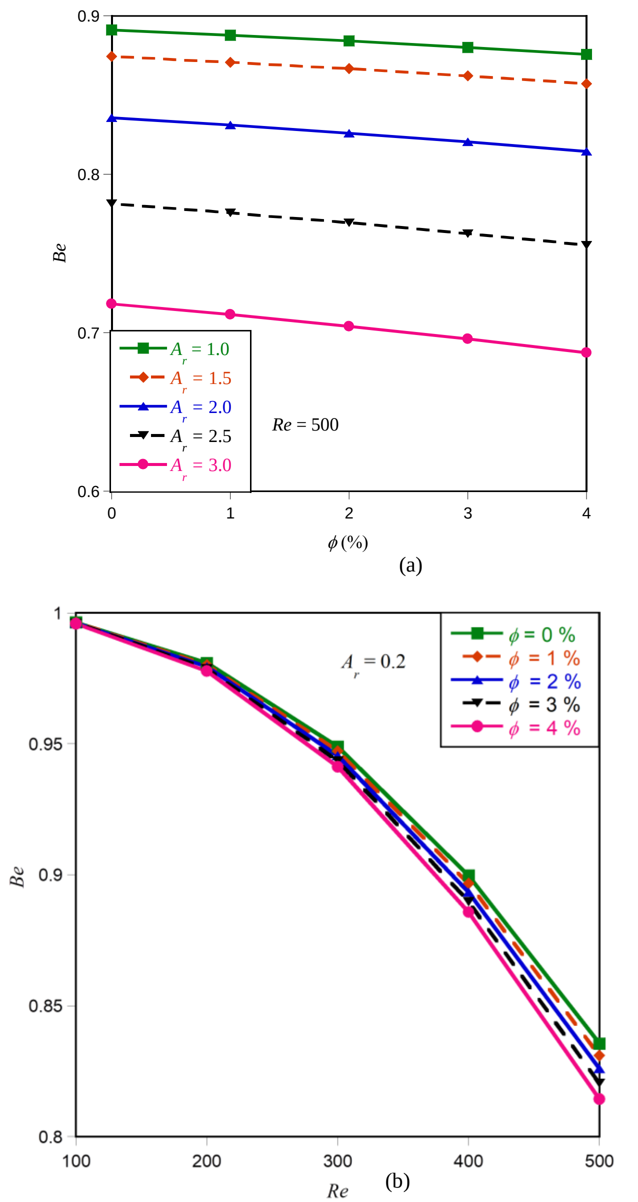

Figure 6: Effect of (a) ϕ at fixed *Re* = 500 and different A_r and (b) Re at fixed A_r = 2 and different ϕ on Be.

E. Influence of ϕ, Re and A_r on Friction Factor

Figure 8 represents the impact of *Re* on the friction factor, *f*, for various nanoparticle concentrations and channel aspect ratios A_r.Figure 8(a) displayed that at specified *Re* = 500, the friction factor remains constant for different values of ϕ while it increases as the A_r increases. This means the *f* is not sensitive to the nanofluid as a coolant for this configuration. Figure 8(b) demonstrates that at fixed A_r = 3, the *f* decreases as the *Re* increases from 100 to 500 for different values of ϕ (Azizi *et al.*, 2016). This decreasing *f* with increasing *Re* is attributed to the increase in inertial force as the *Re* increases as compared with the viscous force of the working fluid (Lodhi *et al.*, 2020).

In Figure 8(a), the constant *f* at each *Re* with varying ϕ in the elliptical cooling microchannel flow is shown. As the ϕ increases the *f* at each of the *Re* remains the same. This behaviour with the circulation of Al_2O_3-water nanofluid at this low concentration serves as a thermal-performance advantage in elliptical cooling microchannels. This is because microchannels are often characterized by higher pressure drops (Byrne *et al.*, 2012, Behi *et al.*, 2020).

The implication of this *f* independence at low concentration of nanofluid is the avoidance of higher pressure drop penalty at low concentration (Zhang *et al.*, 2013), as the size of the particles is small. This pattern is similar to the results obtained in the work of Byrne *et al.* (2012) and Zhang *et al.* (2013). In the work of Byrne *et al.* (2012) CuO nanofluid with seven different concentrations was circulated in a parallel microchannel layout. They found that in each mass flow rate, the pressure remains constant for the seven different nanofluid concentrations for both circular and triangular microchannels. The independence of *f* with a varying ϕ, of the Al_2O_3 nanofluid makes the nanofluid behave like a single-phase fluid. A similar *f* characteristic was obtained in the work of Lee and Mudawar (2007) conducted on the single- and two-phase nanofluids heat transfer in microchannels.

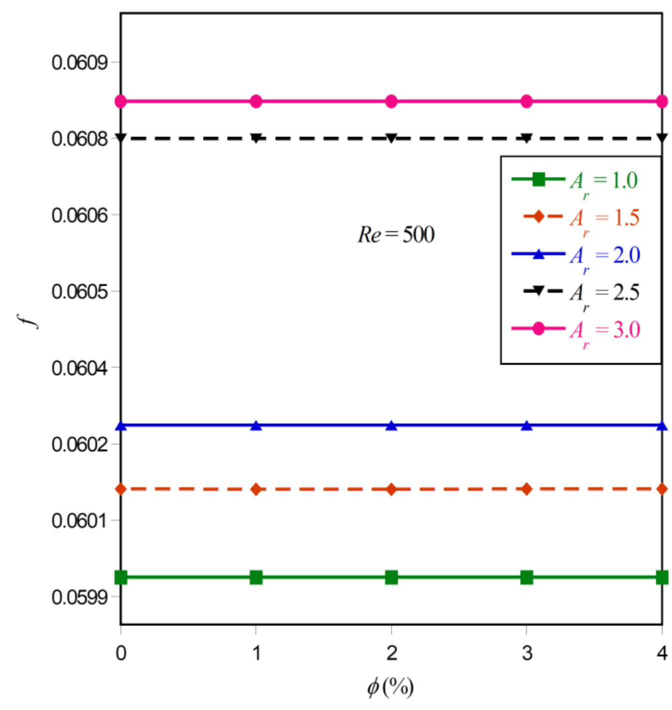

(a)

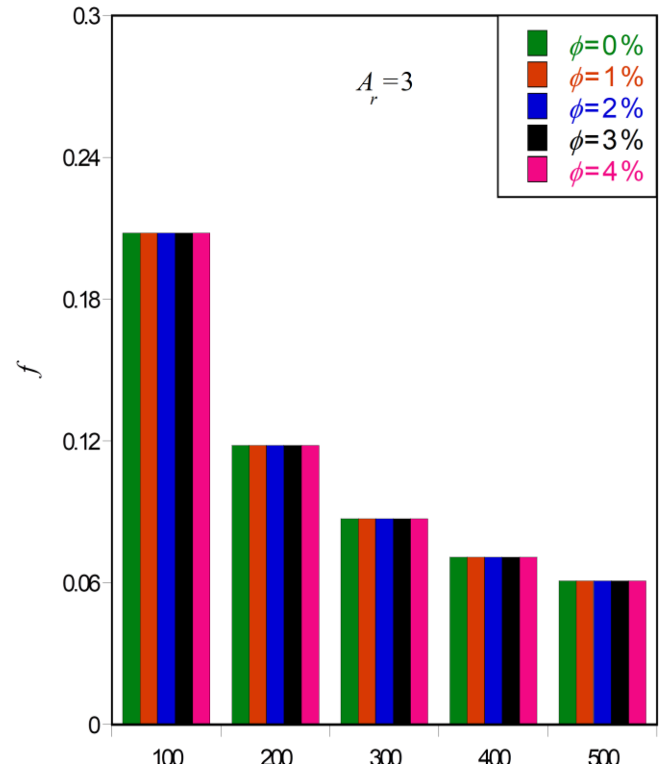

(b)

Figure 8: Effect of ϕ and on the friction factor at fixed *Re* = 500 and different A_r

VIII. CONCLUSION

This research presents a numerical analysis of a three-dimensional elliptical microchannel heat sink for heat dissipation in laminar forced convection with Al_2O_3-water nanofluid. The solid structure experiences internal heat generation within it. The influence of Reynolds number (*Re*), nanofluid concentration (ϕ), and aspect ratio (A_r) on the maximum temperature (T_{max}), average heat transfer coefficient, friction factor, and volumetric entropy generation are carefully studied. The study establishes that heat transfer is significantly enhanced in the elliptical cooling channel at different aspect ratios, nanoparticle concentrations, and Reynold numbers. The results indicate that as the ϕ, A_r and *Re* increase, the maximum temperature, and total entropy generation decrease while the heat transfer coefficient increases. Also, the friction factor increases as the A_r and *Re* increase; however, there is no significant influence of Al_2O_3-water nanofluid on friction factor with an increase in nanofluid concentration. This study establishes that when designing the microchannel heat sink of elliptical channel configurations, channel aspect ratio and fluid thermal properties are very significant parameters to be considered to achieve efficient performance of the cooling channel.

AUTHOR CONTRIBUTIONS

O. T. Olakoyejo: Conceptualization, Methodology, Investigation, Software, Validation, Discussion of results, Writing – original draft, Writing – review & editing, Supervision. **A. O. Adelaja:** validation, Discussion of results, Writing – original draft, Writing – review & editing, Supervision. **S. M. Abolarin:** Conceptualization, Discussion of results: Writing – original draft, Writing – Review and Editing, Supervision**. O. O. Adewumi:** Methodology, Investigation, Software, Validation, Discussion of results, Writing – review & editing. **M. O. Oyekeye:** Methodology, Investigation, Validation, Discussion of results, Writing – review and editing, **A. A. Oluwo:** Software, Validation, Discussion of results, Writing – review & editing. **O. Oluwatusin:** Discussion of results, writing – original draft, Writing – review & editing. . **A. Mweigye:** Methodology, Investigation, Software, Validation, Writing – review & editing, Supervision.

ACKNOWLEDGEMENTS

The authors appreciate the support of the University of the Free State, South Africa, and the University of Lagos, Nigeria.

REFERENCES

Abbas, Z.; M. Naveed; M. Hussain and N. Salamat (2020). Analysis of entropy generation for MHD flow of viscous fluid embedded in a vertical porous channel with thermal radiation. Alexandria Engineering Journal, 59(5): 3395-3405.

Adewumi, O. O.; T. Bello-Ochende and J. P. Meyer (2013). Constructal design of combined microchannel and micro pin fins for electronic cooling. International Journal of Heat and Mass Transfer, 66: 315-323.

Alfaryjat, A. A.; H. A. Mohammed; N. M. Adam, D. Stanciu and A. Dobrovicescu (2018). Numerical investigation of heat transfer enhancement using various nanofluids in hexagonal microchannel heat sink', Thermal Science and Engineering Progress, 5: 252-262.

Alfaryjat, A. A; D. Stanciu; A. Dobrovicescu; V. Badescu and M. Aldhaidhawi (2016). Numerical investigation of entropy generation in microchannels heat sink with different shapes. IOP Conference Series: Materials Science and Engineering, 147: 012134.

Alzahrani, F. and Ijaz Khan, M. (2022). Entropy generation and Joule heating applications for Darcy Forchheimer flow of Ree-Eyring nanofluid due to double rotating disks with artificial neural network. Alexandria Engineering Journal, 61(5): 3679-3689.

Ansys 'Academic Research Mechanical. ANSYS Inc, Release 19.2.

Awad, M. M. (2015). A review of entropy generation in microchannels. Advances in Mechanical Engineering, 7(12): 1687814015590297.

Azizi, Z.; A. Alamdari and Malayeri, M. R. (2016). Thermal performance and friction factor of a cylindrical microchannel heat sink cooled by Cu-water nanofluid. Applied Thermal Engineering, 99: 970-978.

Bahiraei, M. and Heshmatian, S. (2018). Thermal performance and second law characteristics of two new microchannel heat sinks operated with hybrid nanofluid containing graphene–silver nanoparticles. Energy Conversion and Management, 168: 357-370.

Behi, M.; M. Shakorian-Poor; S. A. Mirmohammadi; H. Behi, J. I. Rubio; N. Nikkam; M. Farzaneh-Gord; Y. Gan and M. Behnia. (2020). Experimental and numerical investigation on hydrothermal performance of nanofluids in micro-tubes. Energy, 193: 116658.

Belhadj, A.; R. Bouchenafa and R. Saim. (2018). Numerical investigation of forced convection of nanofluid in microchannels heat sinks. Journal of Thermal Engineering, 4: 2263 - 2273.

Bello-Ochende, T.; L. Liebenberg and J. P. Meyer. (2007). Constructal cooling channels for micro-channel heat sinks. International Journal of Heat and Mass Transfer, 50(21): 4141-4150.

Bello-Ochende, T.; J. P. Meyer and F. U. Ighalo. (2010). Combined numerical optimization and constructal theory for the design of microchannel heat sinks. Numerical Heat Transfer, Part A: Applications, 58(11): 882-899.

Bianco, V.; O. Manca and S. Nardini. (2014). Performance analysis of turbulent convection heat transfer of Al2O3 water-nanofluid in circular tubes at constant wall temperature. Energy, 77: 403-413.

Byrne, M. D.; R. A. Hart and A. K. Da Silva. (2012). Experimental thermal–hydraulic evaluation of CuO nanofluids in microchannels at various concentrations with and without suspension enhancers. International Journal of Heat and Mass Transfer, 55(9): 2684-2691.

Cai, M.; P. Cui; Y. Qin; D. Geng; Q. Wei; X. Wang; D. Yang and G. Zhang. (2020). Entropy Generation Methodology for Defect Analysis of Electronic and Mechanical Components—A Review. Entropy, 22(2): 254.

Chein, R. and Chuang, J. (2007). Experimental microchannel heat sink performance studies using nanofluids. International Journal of Thermal Sciences, 46(1): 57-66.

Choi, S. U. S. and Eastman, J. (1995). Enhancing thermal conductivity of fluids with nanoparticles. In: D. A. Siginer and H. P. Wang, Eds., Developments and Applications of Non-Newtonian Flows, 66: 99-105.

Das, S. K.; N. Putra; P. Thiesen and W. Roetzel (2003). Temperature dependence of thermal conductivity enhancement for nanofluids. Journal of Heat Transfer, 125(4): 567-574.

Dong, T. (2019). Chapter 3 - Thermohydrodynamics for single-phase convection in microchannel networks', in T. Dong (ed)^(eds). Thermohydrodynamic Programming and Constructal Design in Microsystems, Academic Press.

Ebrahimi, A.; F. Rikhtegar; A. Sabaghan and E. Roohi. (2016). Heat transfer and entropy generation in a microchannel with longitudinal vortex generators using nanofluids. Energy, 101: 190-201.

Fadodun, O. G.; D. R. E. Ewim and S. M. Abolarin (2022). Investigation of turbulent entropy production rate with SWCNT/H2O nanofluid flowing in various inwardly corrugated pipes. Heat Transfer: 1-28.

Hajmohammadi, M. R. and I. Toghraei. (2018). Optimal design and thermal performance improvement of a double-layered microchannel heat sink by introducing Al2O3 nano-particles into the water. Physica A: Statistical Mechanics and its Applications, 505: 328-344.

Hassan, M.; R. Sadri; G. Ahmadi; M. B. Dahari; S. N. Kazi; M. R. Safaei and E. Sadeghinezhad. (2013). Numerical study of entropy generation in a flowing nanofluid used in micro- and minichannels. Entropy, 15(1): 144-155.

Ibrahim, W.; D. Gamachu and B. Bedada. (2022). Entropy generation analysis of three dimensional mixed convection flow of couple stress nanofluid with non-Fourier's heat and non-Fick's mass flux model. Alexandria Engineering Journal, 61(11): 8843-8857.

Jing, D.; S. Song; Y. Pan and X. Wang. (2018). Size dependences of hydraulic resistance and heat transfer of fluid flow in elliptical microchannel heat sinks with boundary slip. International Journal of Heat and Mass Transfer, 119: 647-653.

Kalteh, M.; A. Abbassi; M. Saffar-Avval; A. Frijns; A. Darhuber and J. Harting. (2012). Experimental and numerical investigation of nanofluid forced convection inside a wide microchannel heat sink. Applied Thermal Engineering, 36: 260-268.

Lee, J. and Mudawar, I. (2007). Assessment of the effectiveness of nanofluids for single-phase and two-phase heat transfer in micro-channels. International Journal of Heat and Mass Transfer, 50(3): 452-463.

Lee, S.; S. U.-S. Choi; S. Li and J. A. Eastman. (1999). Measuring thermal conductivity of fluids containing oxide nanoparticles. Journal of Heat Transfer, 121(2): 280-289.

Li, X. F.; D. S. Zhu; X. J. Wang; N. Wang; J. W. Gao and H. Li. (2008). Thermal conductivity enhancement dependent pH and chemical surfactant for Cu-H_2O nanofluids. Thermochimica Acta, 469(1): 98-103.

Lodhi, M. S.; T. Sheorey and G. Dutta. (2020). Single-phase fluid flow and heat transfer characteristics of nanofluid in a circular microchannel: Development of flow and heat transfer correlations. Proceedings of the Institution of Mechanical Engineers, Part C: Journal of Mechanical Engineering Science, 234(18): 3689-3708.

Manay, E.; E. F. Akyürek and B. Sahin. (2018). Entropy generation of nanofluid flow in a microchannel heat sink. Results in Physics, 9: 615-624.

Mardani, M. and Salimpour, M. R. (2016). Optimization of triangular microchannel heat sinks using constructal theory. Journal of Mechanical Science and Technology, 30(10): 4757-4764.

Meyer, J. P.; O. T. Olakoyejo and T. Bello-Ochende. (2012). Constructal optimisation of conjugate triangular cooling channels with internal heat generation. International Communications in Heat and Mass Transfer, 39(8): 1093-1100.

Muzychka, Y. S. (2007). Constructal multi-scale design of compact micro-tube heat sinks and heat exchangers. International Journal of Thermal Sciences, 46(3): 245-252.

Naz, R.; M. Noor; Z. Shah; M. Sohail; P. Kumam and P. Thounthong. (2020). Entropy generation optimization in MHD pseudoplastic fluid comprising motile microorganisms with stratification effect. Alexandria Engineering Journal, 59(1): 485-496.

Nguyen, C. T.; G. Roy; C. Gauthier and N. Galanis. (2007). Heat transfer enhancement using Al2O3–water nanofluid for an electronic liquid cooling system. Applied Thermal Engineering, 27(8): 1501-1506.

Olakoyejo, O. T. (2012). Geometric optimisation of conjugate heat transfer in cooling channels with different cross-sectional shapes. Department of Mechanical and Aeronautical Engineering, University of Pretoria, Pretoria.

Olakoyejo, O. T.; T. Bello-Ochende and J. P. Meyer. (2012a). Constructal conjugate cooling channels with internal heat generation. International Journal of Heat and Mass Transfer, 55(15): 4385-4396.

Olakoyejo, O. T.; T. Bello-Ochende and J. P. Meyer. (2012b). Mathematical optimisation of laminar forced convection heat transfer through a vascularised solid with square channels. International Journal of Heat and Mass Transfer, 55(9): 2402-2411.

Pak, B. C. and Cho, Y. I. (1998). Hydrodynamic and heat transfer study of dispersed fluids with submicron metallic oxide particles. Experimental Heat Transfer, 11(2): 151-170.

Palm, S. J.; G. Roy and Nguyen, C. T. (2006). Heat transfer enhancement with the use of nanofluids in radial flow cooling systems considering temperature-dependent properties. Applied Thermal Engineering, 26(17): 2209-2218.

Patankar, S. V. (1980). Numerical heat transfer and fluid flow, CRC Press.

Riaz, A.; S. Almutairi; S. E. Alhazmi; A. Saleem; S. Nadeem and A. Abdelrahman. (2022). Insight into the cilia motion of electrically conducting Cu-blood nanofluid through a uniform curved channel when entropy generation is significant. Alexandria Engineering Journal, 61(12): 10613-10630.

Salawu, S. O.; A. R. Hassan; A. Abolarinwa and N. K. Oladejo. (2019). Thermal stability and entropy generation of unsteady reactive hydromagnetic Powell-Eyring fluid with variable electrical and thermal conductivities. Alexandria Engineering Journal, 58(2): 519-529.

Salimpour, M. R.; A. T. Al-Sammarraie; A. Forouzandeh and M. Farzaneh. (2018). Constructal design of circular multilayer microchannel heat sinks. Journal of Thermal Science and Engineering Applications, 11(1): TSEA-18-1006 - 011001.

Salimpour, M. R.; M. Sharifhasan and E. Shirani. (2011). Constructal optimization of the geometry of an array of micro-channels. International Communications in Heat and Mass Transfer, 38(1): 93-99.

Shi, X.; S. Li; Y. Wei and J. Gao. (2018). Numerical investigation of laminar convective heat transfer and pressure drop of water-based Al2O3 nanofluids in a microchannel. International Communications in Heat and Mass Transfer, 90: 111-120.

Siginer, D. A. and Wang, **H.-P.** Developments and applications of non-Newtonian flows, (ed)^(eds), Presented at the 1995 ASME International Mechanical Engineering Congress and Exposition, San Francisco, California, ASME.

Souayeh, B.; F. Hammami; N. Hdhiri; M. W. Alam; E. Yasin and A. Abuzir. (2021). Simulation of natural convective heat transfer and entropy generation of nanoparticles around two spheres in horizontal arrangement. Alexandria Engineering Journal, 60(2): 2583-2605.

Teng, T.-P.; Y.-H. Hung; T.-C. Teng; H.-E. Mo and H.-G. Hsu. (2010). The effect of alumina/water nanofluid particle size on thermal conductivity. Applied Thermal Engineering, 30(14): 2213-2218.

Tsuda, S.; M. Shimizu; F. Iguchi and H. Yugami. (2017). Enhanced thermal transport in polymers with an infrared-selective thermal emitter for electronics cooling. Applied Thermal Engineering, 113: 112-119.

Tuckerman, D. B. and Pease, R. F. W. (1981). High-performance heat sinking for VLSI. IEEE Electron Device Letters, 2(5): 126-129.

Vajjha, R. S. and Das, D. K. (2009). Experimental determination of thermal conductivity of three nanofluids and development of new correlations. International Journal of Heat and Mass Transfer, 52(21): 4675-4682.

Wang, X., X. Xu and S. U. S. Choi. (1999). Thermal conductivity of nanoparticle - fluid mixture', Journal of Thermophysics and Heat Transfer, 13(4): 474-480.

Wei Ting, T.; Y. Mun Hung and N. Guo (2016). Viscous dissipation effect on streamwise entropy generation of nanofluid flow in microchannel heat sinks. Journal of Energy Resources Technology, 138(5): JERT-14-1311 - 052002.

Xuan, Y. and Li, Q. (2003). Investigation on convective heat transfer and flow features of nanofluids. Journal of Heat Transfer, 125(1): 151-155.

Yang, Y.; Z. G. Zhang; E. A. Grulke; W. B. Anderson and G. Wu. (2005). Heat transfer properties of nanoparticle-in-fluid dispersions (nanofluids) in laminar flow. International Journal of Heat and Mass Transfer, 48(6): 1107-1116.

Yue, Y.; S. K. Mohammadian and Y. Zhang. (2015). Analysis of performances of a manifold microchannel heat sink with nanofluids. International Journal of Thermal Sciences, 89: 305-313.

Zhang, H.; X. Nie; D. O. Bokov; D. Toghraie; O. A. Akbari; F. Montazerifar; F. Pourfattah; Y. Esmaeili and R. Khodaparast. (2022). Numerical study of mixed convection and entropy generation of Water-Ag nanofluid filled semi-elliptic lid-driven cavity. Alexandria Engineering Journal, 61(11): 8875-8896.

Zhang, H.; S. Shao; H. Xu and C. Tian. (2013). Heat transfer and flow features of Al2O3–water nanofluids flowing through a circular microchannel – Experimental results and correlations. Applied Thermal Engineering, 61(2): 86-92.